Kiminori Fujimoto, MD, PhD
Toshi Abe, MD, PhD
Nestor L. Müller, MD, PhD
Hiroshi Terasaki, MD
Seiya Kato, MD, PhD
Junko Sadohara, MD
Rei Kono, MD
Osamu Edamitsu, MD, PhD
Tatsuya Ishitake, MD, PhD
Akihiro Hayashi, MD, PhD
Toru Rikimaru, MD, PhD
Naofumi Hayabuchi, MD, PhD

Index terms:
Lung neoplasms, 60.31
Lung neoplasms, diagnosis
Lung neoplasms, MR, 60.12143, 60.12144

Published online before print
10.1148/radiol.2273020459
Radiology 2003; 227:786–793

Abbreviations:
MER = maximum enhancement ratio
MVDG = microvessel density grade
SI = signal intensity
SI_{max} = SI at T_{max}
SI_{prior} = SI before injection
SI_{WR} = SI at 3 minutes after T_{max}
T_{max} = time lapse between the completion of the injection and the point of maximum SI
VEGF = vascular endothelial growth factor

[1] From the Depts of Radiology (K.F., T.A., H.T., J.S., R.K., O.E., N.H.), Pathology (S.K.), Environmental Medicine (T.I.), and Surgery (A.H.) and First Dept of Internal Medicine (T.R.), Kurume Univ School of Med, 67 Asahimachi, Kurume, Fukuoka 830-0011, Japan; and Dept of Radiology, Vancouver Gen Hosp, Univ of British Columbia, Canada (N.L.M.). From the 2001 RSNA scientific assembly. Received Apr 18, 2002; revision requested Jun 19; final revision received Nov 4; accepted Nov 27. **Address correspondence to** K.F. (e-mail: *kimichan@med.kurume-u.ac.jp*).

Author contributions:
Guarantors of integrity of entire study, K.F., T.A., N.H.; study concepts, K.F.; study design, K.F., T.A.; literature research, K.F., T.A., N.L.M.; clinical studies, H.T., J.S., R.K., A.H., T.R.; data acquisition, K.F., T.A.; data analysis/interpretation, K.F., T.I.; statistical analysis, K.F., T.I.; manuscript preparation and editing, K.F., N.L.M.; manuscript definition of intellectual content, K.F.; manuscript revision/review, all authors; manuscript final version approval, K.F., N.L.M., N.H.

Small Peripheral Pulmonary Carcinomas Evaluated with Dynamic MR Imaging: Correlation with Tumor Vascularity and Prognosis[1]

PURPOSE: To correlate the findings at contrast material–enhanced dynamic magnetic resonance (MR) imaging of small peripheral pulmonary carcinomas with tumor vascularity and prognosis.

MATERIALS AND METHODS: Ninety-four patients with small peripheral pulmonary carcinomas who underwent surgical resection were examined retrospectively. Pathologic specimens were stained with hematoxylin-eosin and elastin–van Gieson. CD34 and vascular endothelial growth factor (VEGF) were assessed immunohistochemically. Delineated CD34-positive cells were counted as microvessels. Dynamic MR imaging was performed prior to and at 1, 2, 3, 4, 5, 6, and 8 minutes after injection of a bolus of gadopentetate dimeglumine. The two observers reviewed all images, and two pathologists performed all histologic analyses; a decision was determined with consensus. The maximum enhancement ratio (MER), the time lapse between the completion of the injection and the point of maximum signal intensity (T_{max}), the washout ratio, and the slope value of the time–signal intensity curve were correlated with the microvessel density. VEGF-positive and VEGF-negative tumors were compared. All statistical analyses were performed by using nonparametric methods.

RESULTS: The MER and the slope value were positively correlated, and the T_{max} was negatively correlated (Spearman rank test, $P < .0001$, all comparisons) with the microvessel counts. The distribution of elastic and collagen fibers correlated with the washout ratio (Kruskal-Wallis test, $P < .001$). There was a statistically significant difference between the slope value of VEGF-positive tumors and that of VEGF-negative tumors (Mann-Whitney U test, $P < .0001$). Patients with VEGF-positive tumors had a significantly shorter overall survival than did those with VEGF-negative tumors (log-rank test, $P < .0001$).

CONCLUSION: Dynamic MR imaging findings correlate with tumor vascularity and may be helpful in the prediction of prognosis.

Findings in recent studies indicate that enhancement of malignant solitary pulmonary nodules following intravenous administration of contrast material is greater than that of benign solitary pulmonary nodules depicted on computed tomographic (CT) scans and magnetic resonance (MR) images (1–11). In the studies, only the maximum enhancement of a solitary pulmonary nodule was evaluated, which is the first half of the time-attenuation or time-signal intensity (SI) curve (the inflow of contrast material to a solitary pulmonary nodule); the latter half (the washout of contrast material from a solitary pulmonary nodule) remains largely uninvestigated.

Recently, it has been shown that histologic assessment of tumor microvessel density and expression of vascular endothelial growth factor (VEGF) are important prognostic factors

in non-small cell lung cancers (12–23). It has also been reported that contrast enhancement at CT and MR imaging correlates with measurements of tumoral microvessel density grade (MVDG) and microvessel counts, that is, tumor angiogenesis (3,4,24,25). The role of MR imaging has been limited to the assessment of differences in SI characteristics of benign and malignant nodules (7–11). We postulated that evaluation of dynamic MR images following intravenous administration of contrast material would correlate with tumor angiogenesis and therefore would be helpful in the prediction of the prognosis. The aim of this study was to correlate the findings at contrast material–enhanced dynamic MR imaging of small peripheral pulmonary carcinomas with tumor vascularity and prognosis.

MATERIALS AND METHODS

Patients

Between 1991 and 1998, we retrospectively reviewed the records of 94 patients who had undergone gadopentetate dimeglumine–enhanced dynamic MR imaging within 2 weeks before surgical resection of a peripheral pulmonary carcinoma that was 3 cm or smaller in largest diameter. Our institutional review board does not require its approval or informed consent for review of a patient's records, files, and images.

The patients ranged in age from 44 to 81 years (mean age, 65.6 years); 56 were men and 38 were women. All patients underwent diagnostic procedures before surgery, and these procedures included brain CT or MR imaging, whole-body CT, and bone scintigraphy. Each patient had one peripheral pulmonary carcinoma; 67 had adenocarcinoma and 27 had squamous cell carcinoma. The 94 pulmonary carcinomas ranged from 1.0 to 3.0 cm (mean, 2.4 cm) in diameter. Sixty-four patients had stage IA cancer, 11 patients had stage IIA cancer, and 19 patients had stage IIIA cancer (26). Findings were negative for lymph node metastasis in 64 patients, and they were positive for lymph node metastasis in 30 patients. The pathologic N factor was N0 in 64 patients, N1 in 11 patients, and N2 in 19 patients.

Dynamic MR Imaging Studies

All MR images were obtained with a 0.5-T superconducting system (Magnex 50HP; Shimadzu, Kyoto, Japan). The dynamic studies were performed with a T1-weighted spin-echo sequence (150/10 repetition time msec/echo time msec, one signal acquired) during breath hold at full inspiration. Three oblique sagittal or transverse images that included the center of the tumor and excluded the heart and great vessels were chosen for the dynamic MR imaging study to avoid cardiac and arterial motion artifacts. A section thickness of 8 mm and a section interval of 10 mm were chosen to maintain a sufficient signal-to-noise ratio, and a 256 × (256 × 0.8) rectangular matrix, a 30 × 30-cm field-of-view, and one signal acquired were used. The sampling time per image was 16 seconds. After the first spin-echo sequence, a manual injection of a bolus of 0.1 mmol per kilogram of body weight of gadopentetate dimeglumine (Magnevist; Schering, Berlin, Germany) was administered intravenously with a 21-gauge butterfly infusion set (Hakko Shoji, Tokyo, Japan) during 10 seconds. The injection was administered by using a small syringe and a stopwatch to ensure even injection of contrast material throughout the 10 seconds. Postcontrast dynamic MR images were obtained at 1, 2, 3, 4, 5, 6, and 8 minutes after completion of the intravenous injection (Fig 1a).

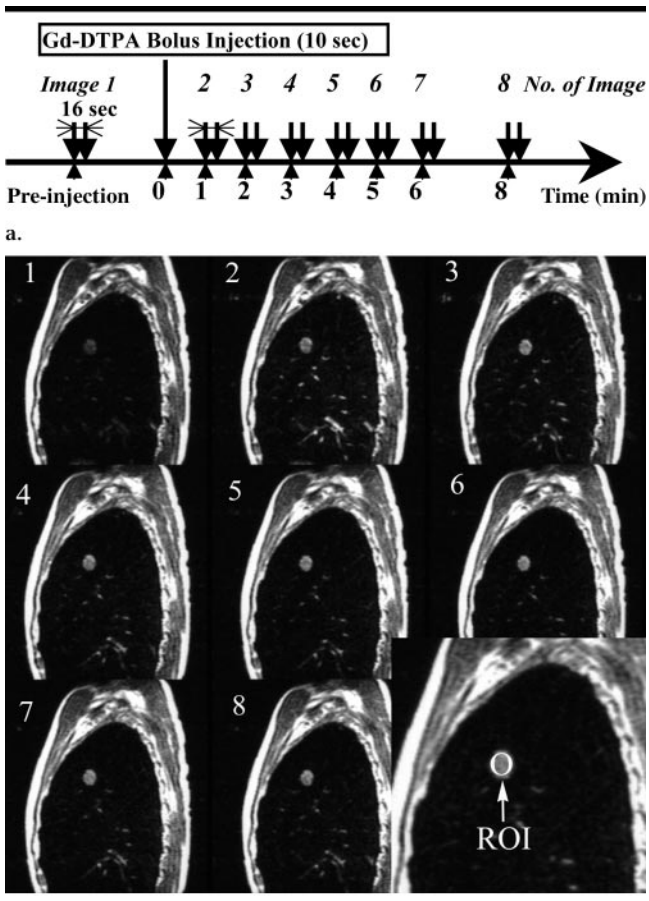

Figure 1. **(a)** Dynamic MR imaging enhancement protocol. After analysis of unenhanced spin-echo MR images obtained through the nodule in the lung, a bolus of 0.1 mmol of gadopentetate dimeglumine *(Gd-DTPA)* per kilogram of body weight was injected intravenously for 10 seconds. Actual sampling time was 16 seconds, and eight images were obtained. **(b)** Sagittal oblique gadopentetate dimeglumine–enhanced dynamic MR images (150/10) obtained in a 67-year-old man with squamous cell carcinoma of the upper lobe of the left lung. This nodule was 22 × 24 mm in diameter. Note placement of region of interest *(ROI)*.

Image Analysis

Two observers (H.T., J.S.) who had no knowledge of the patients' clinical or histologic data reviewed all images and determined a decision with consensus.

Tumor enhancement on the dynamic

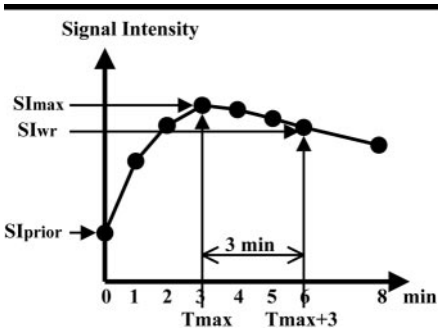

Figure 2. Graph shows time-SI curve. Gadopentetate dimeglumine was the contrast agent used.

spin-echo images was measured with stand-alone software (Time-Intensity Curve; Shimadzu). The SI of the tumor was measured on circular operator-defined regions of interest (Fig 1b) with an electronic cursor on each spin-echo image. All of the regions of interest were placed by the same two observers with consensus. Large regions of interest were chosen to incorporate solid-appearing parts of a tumor and exclude obvious cystic or necrotic areas, as described by Swensen et al (1) and Yamashita et al (2). Time-SI curves were obtained for the values derived from each image plotted against time; the SI before injection (SI_{prior}), the time lapse between the completion of the injection and the point of maximum SI (T_{max}), and the SI at T_{max} (SI_{max}) were determined for each image (Fig 2).

The enhancement ratio at T_{max} (maximum enhancement ratio [MER]) was calculated as the percentage of increase of the SI between the SI_{prior} and the SI_{max} as follows: $MER = (SI_{max} - SI_{prior}) \times 100/SI_{prior}$ (percent). When the rate of increase of SI toward the peak was less than 3%, MER was defined as the peak of the time-SI curve or as before the point of the peak (27). The slope value of the time-SI curve was calculated as the percentage of increase of the SI at the T_{max} over the baseline value per minute with the following equation: $slope = (SI_{max} - SI_{prior}) \times 100/(SI_{prior} \times T_{max}) = MER/T_{max}$ (percent per minute). The washout ratio, or WR, was calculated as the percentage of decrease of the SI between the SI_{max} and the SI at 3 minutes after T_{max} (SI_{WR}) with the following equation: $WR = (SI_{max} - SI_{WR}) \times 100/SI_{max}$ (percent). When the T_{max} of the time-SI curve was 4 minutes, the SI_{WR} was directly obtained from the time-SI curve because the image at 7 minutes was not obtained. When the T_{max} was at 6 or 8 minutes, the washout ratio could not be calculated according to the definition of the washout ratio. Therefore, the washout ratio of such cases was set at zero.

Histologic Examination

Two pathologists (S.K., O.E.) without any information about the radiologic images and patient characteristics performed all histologic analyses and determined a decision with consensus. The analysis was performed on archived sections.

All surgical specimens were fixed with 10% buffered formalin in the inflated state by means of transpleural and transbronchial injection of 10% formalin for 24 hours. The pathologic specimens were sectioned transversely or coronally at 5-mm intervals in the same plane in which the dynamic MR images were obtained. Histologic materials including the tumor were embedded in paraffin wax. Two-micrometer sections were stained with hematoxylin-eosin for the conventional histologic characterization of lesions and with elastin–van Gieson for the analysis of the tumor interstitium. The other series of sections were used for the immunohistochemical analysis with a staining kit (LSAB; Dako Japan, Kyoto, Japan). For the detection of VEGF, the section was incubated with a 1:50 dilution of rabbit polyclonal antibody against a peptide mapping at the amino terminus of human VEGF (A-20; Santa Cruz Biotech, Santa Cruz, Calif). For the detection of CD34, the section was autoclaved for 2 minutes at 121°C in a 0.05M (0.05 mol/L) citrate buffer (pH 6.0) for the antigen retrieval and then incubated with a 1:50 dilution of mouse monoclonal antibody for human CD34 class I (BL-3C5; Dako Japan). The primary antibodies were incubated at 4°C overnight. The section was counterstained with hematoxylin-eosin after the immunodetection. Nonimmunoserum or a blocking peptide against CD34 antibody (sc152P; Santa Cruz Biotech) was used for the negative control.

Evaluation of MVDG and microvessel counts were assessed as previously described by Weidner et al (28) and Buadu et al (29), with minor modifications. Briefly, any CD34-positive endothelial cell or cell cluster that was clearly separate from adjacent tumor cells and other connective tissue elements was considered to be a single countable microvessel. Vessel lumen was usually recognized inside of the vessel; however, it was not necessary for the structural definition of the microvessel. We did not use the presence of red blood cells to define a vessel lumen. All of the specimens were imaged at low magnification (×40 or ×100), and the area of the densest neovascularization (greatest number of capillaries or small vessels) was first identified at imaging of the tumor sections. This neovascularization was then subjectively graded on a scale of 1+ (MVDG 1), which indicated low density of neovascularization, to 3+ (MVDG 3), which indicated high density of neovascularization. Individual microvessel counts were determined with a ×200 microscopic field, or 0.949 mm^2 per field, in the five areas of the highest vascular density. The microvessel counts were expressed as the mean counts in these five areas.

Distribution of the tumor interstitium was assessed by using the method of Yamashita et al (3). Elastic fibers and collagen fibers are the main components of the extracellular matrix of the normal lung, and the pulmonary interstitium is composed of these fibers. With the elastin–van Gieson method, elastic fibers are stained dark brown and collagen fibers are stained pink. Accordingly, at staining with the elastin–van Gieson method, distributions of elastic fibers and collagen fibers were evaluated and graded as follows: elastic fibers 1 or collagen fibers 1, elastic fibers or collagen fibers in less than 20% of the inner area of the tumor; elastic fibers 2 or collagen fibers 2, elastic fibers or collagen fibers in more than 20% and less than 40% of the inner area of the tumor; and elastic fibers 3 or collagen fibers 3, elastic fibers or collagen fibers in more than 40% of the inner area of the tumor. The distribution of elastic fibers and collagen fibers (elastic fibers 1–3 and collagen fibers 1–3) was randomly evaluated five times with a ×200 microscopic field in the same inner area of the tumor as was used for calculation of the microvessel counts, and the median grade was chosen.

VEGF was considered positive if there was unequivocal immunostaining of the membrane or cytoplasm in more than 5% of the tumor cells on the slide of the largest section of the tumor, as reported by Tomoda et al (30).

Statistical Analysis

Normality was evaluated by using the Shapiro-Wilk test. Because only the continuous variable of the slope value was normally distributed, nonparametric methods were used.

The relationship between VEGF expres-

TABLE 1
Correlation between Microvessel Counts and Enhancement Characteristics

Characteristic	Spearman *r*	*P* Value
MER	0.469	<.0001
T_{max}	−0.693	<.0001
Slope	0.739	<.0001
Washout ratio	0.251	.015

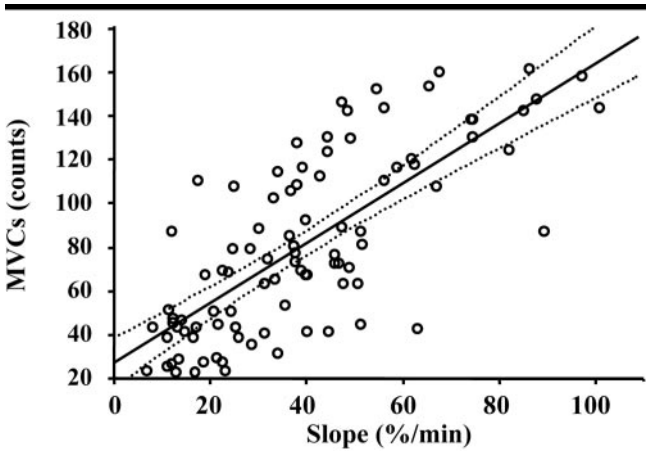

Figure 3. Graph shows the relationship between the slope and microvessel counts *(MVCs)*. Slope was positively correlated with the microvessel counts (y = 27.382 + 1.372x; $r^2 = 0.563$; $P < .0001$).

sion and patient characteristics, pathologic characteristics (tumor histologic type, microvessel counts, MVDG, and density grade of tumor interstitium; elastic fibers 1-3 or collagen fibers 1-3), or each parameter of dynamic MR imaging (MER, T_{max}, slope, or washout ratio), and the relationship between the microvessel counts or MVDG and elastic fibers 1–3 or collagen fibers 1–3 were determined by using the χ^2 test and the Mann-Whitney *U* test. The correlation between the microvessel counts and each parameter of dynamic MR imaging was analyzed by using the Spearman rank correlation coefficient (Spearman *r*). The linear regression between the microvessel counts and MR imaging parameters was performed with stepwise multiple regression analysis. The statistical analyses of the correlation of each parameter of dynamic MR imaging with MVDG and elastic fibers 1–3 or collagen fibers 1–3 were performed by using the Kruskal-Wallis and Bonferroni tests.

All patients had been followed up for a minimum of 24 months (median follow-up, 60 months; range, 24–124 months) at the time of the final observation (August 2000) or at death. Survival was calculated from date of surgery to date of death or last contact. In the latter group, survival was calculated by using a right censoring survival model. Survival outcomes were obtained from the patients' medical records or from the records of their primary care physicians or surgeons. The survival curves were calculated by using the Kaplan-Meier method and were analyzed by using the log-rank test. The effect of each variable on the risk of death was assessed with multivariate analyses by using the Cox proportional hazards model.

A *P* value of less than .05 was considered to indicate a statistically significant difference. The Shapiro-Wilk test was performed with statistical software (JMP, version 4.0; SAS, Cary, NC). All other statistical analyses were performed with software (StatView, version 5.0; Abacus Concepts, Berkeley, Calif) and a computer (Macintosh; Apple Computer, Cupertino, Calif).

RESULTS

Relationship between Imaging Parameters and Histologic Findings

There were no statistically significant differences in patient characteristics, individual parameters of dynamic MR imaging, or pathologic findings between patients with adenocarcinoma and those with squamous cell carcinoma. The patients with lymph node metastasis had an earlier T_{max} and higher slope value than did those without metastasis (both, $P < .05$).

The microvessel counts were positively correlated with both the MER (Spearman $r = 0.469$, $P < .0001$) and the slope value ($r = 0.739$, $P < .0001$) and negatively correlated with the T_{max} ($r = -0.693$, $P < .0001$) (Table 1). The stepwise multiple regression analyses revealed that the slope value was independently positively correlated with the microvessel counts (y = 27.382 + 1.372x; $r^2 = 0.564$; $P < .0001$) (Fig 3). The relationship between MVDG and enhancement characteristics (Table 2) revealed that tumors classified in MVDG 3 had a higher MER and slope value and an earlier T_{max} than did tumors classified in MVDG 1 or 2. However, the difference was not significant in regard to the washout ratio of MVDG 1–3.

The washout ratio was influenced by the percentage of elastic fibers and collagen fibers in the tumor interstitium. There were significant differences between elastic fibers 1–3 and the washout ratio and between collagen fibers 1–3 and the washout ratio (Kruskal-Wallis test, elastic fibers 1–3 vs washout ratio, $P < .001$; collagen fibers 1–3 vs washout ratio, $P < .05$). The Bonferroni test revealed that the washout ratio was greater in elastic fibers 1 than it was in elastic fibers 2 and 3 (elastic fibers 1 vs elastic fibers 2 and 3, $P < .01$), and the washout ratio was greater in collagen fibers 1 than it was in collagen fibers 3 ($P < .05$). Other parameters of dynamic MR imaging (MER, T_{max}, and slope value) did not correlate significantly with the percentage of elastic fibers or collagen fibers.

The difference between elastic fibers 1–3 and microvessel counts was significant (Kruskal-Wallis test, $P < .001$); however, the difference between collagen fibers 1–3 and microvessel counts was not statistically significant. The Bonferroni test revealed that the number of microvessel counts in elastic fibers 1 was smaller than that in elastic fibers 2 and 3 (both, $P < .05$).

Relationship between VEGF and Patient Characteristics, MVDG, Microvessel Counts, and Imaging Parameters

The statistically significant differences between VEGF-positive and VEGF-negative tumors are summarized in Tables 3 and 4.

The correlations between VEGF and patients' characteristics (age, sex, and histologic type) did not indicate a significant difference. However, 25 (42%) of 60 patients with VEGF-positive tumors had lymph node metastasis, compared with only five (15%) of 34 patients with VEGF-negative tumors ($P < .01$). There were

TABLE 2
Relationship between MVDG and Enhancement Characteristics

Characteristic	MVDG 1	MVDG 2	MVDG 3	*P* Value*
MER (%)	75.6 (60.0–101.7)	94.8 (84.4–105.3)	113.4 (88.2–138.0)	<.0001
T_{max} (min)	5.0 (3.0–5.0)	3.0 (2.0–3.0)	2.0 (2.0–2.0)	<.0001
Slope (percent per minute)	16.7 (12.2–25.8)	37.4 (28.6–46.3)	58.7 (43.7–74.3)	<.0001
Washout ratio (%)	5.4 (1.7–11.3)	7.5 (4.7–13.7)	8.9 (4.4–12.3)	.1126

Note.—Values other than *P* values are the medians. Values in parentheses are the interquartile ranges (range, 25th to 75th percentile).
* Values were calculated with the Kruskal-Wallis test.

TABLE 3
Relationship between VEGF Expression and Nodal Status and MVDG

Factor	VEGF-Positive Tumors (n = 60)	VEGF-Negative Tumors (n = 34)
Nodal status		
Positive	25 (42)	5 (15)
Negative	35 (58)	29 (85)
MVDG		
1	7 (12)	23 (68)
2	27 (45)	8 (24)
3	26 (43)	3 (9)

Note.—*P* values were calculated with the χ^2 test and were .0071 for nodal status and <.0001 for MVDG. Data are numbers of patients. Data in parentheses are percentages.

TABLE 4
Relationship between VEGF Expression and Microvessel Count and Enhancement Characteristics

Factor	VEGF-Positive Tumors	VEGF-Negative Tumors	*P* Value*
Microvessel Count†	89.5 (68.0–129.0)	44.0 (30.0–69.0)	<.0001
Characteristic			
MER (%)	100.3 (88.5–122.6)	78.3 (64.8–94.9)	<.0001
T_{max} (min)	4.0 (2.0–3.0)	2.0 (3.0–5.0)	<.0001
Slope (percent per minute)	44.9 (35.6–58.0)	19.6 (12.6–28.2)	<.0001
Washout ratio (%)	7.4 (4.3–13.7)	5.9 (2.3–11.8)	.0679

Note.—Values other than *P* values are the medians. Values in parentheses are the interquartile ranges (range, 25th to 75th percentile).
* Values were calculated with the Mann-Whitney *U* test.
† Microvessel counts are number of counts per ×200 microscopic field.

significantly more microvessel counts in patients with VEGF-positive tumors than there were in those with VEGF-negative tumors ($P < .0001$). The MVDG in patients with VEGF-positive tumors was higher than it was in patients with VEGF-negative tumors ($P < .0001$). The MER and the slope value in patients with VEGF-positive tumors were higher than they were in those with VEGF-negative tumors ($P < .0001$), and the T_{max} in patients with VEGF-positive tumors occurred earlier than it did in those with VEGF-negative tumors ($P < .0001$). However, the difference of VEGF expression with washout ratio was not significant ($P = .0709$).

Prognosis

Postoperative survival rates of the patients with tumors are shown in Figures 4–8. At the time of the analysis in this study, 36 patients had died. Overall 5- and 10-year survival rates were 67.5% and 30.6%, respectively.

Patients who had lymph node metastasis had a significantly shorter overall survival than did those with no lymph node metastasis (log-rank test, $P < .0001$).

Patients with VEGF-positive tumors had a significantly shorter overall survival than did those with VEGF-negative tumors ($P < .0001$). Among 64 patients with stage IA (N0) cancer, however, there was no statistically significant overall survival between patients with VEGF-positive tumors and those with VEGF-negative tumors ($P = .098$). Patients with MVDG 1 had a significantly better prognosis than did those with MVDG 2 and 3 (MVDG 1 vs MVDG 2 and 3, $P < .01$). All patients were classified into two groups (a group with higher and a group with lower slope values) according to the cutoff value, which represented the median of all slope values (37.3% per minute). Patients with a higher slope value had a significantly shorter overall survival than did those with a lower slope value ($P < .01$).

The Cox proportional hazards model showed that a VEGF-positive tumor ($P < .05$; risk ratio, 3.254; 95% CI: 1.036, 10.218), the slope value ($P < .01$; risk ratio, 1.036; 95% CI: 1.011, 1.062), and a finding positive for lymph node metastasis ($P < .0001$; risk ratio, 9.676; 95% CI: 4.327, 22.097) were significantly related to survival.

Fifteen (83%) of 18 patients with all three factors, 14 (45%) of 31 patients with two factors, three (15%) of 20 patients with one factor, and four (16%) of 25 patients with none of these factors died during the study period (Fig 8).

DISCUSSION

It has been shown that the degree of enhancement at CT following intravenous administration of contrast material correlates with the number of small vessels (3,4,24) and with endothelial cell markers (7). Yamashita et al (3) correlated the findings at contrast-enhanced dynamic CT with the number of blood vessels and the quantity of the tumoral interstitium (ie, elastic fibers). Maximum attenuation of lung carcinomas correlated with the number of small vessels (diameter, 0.02–0.10 mm) as assessed by using the factor VIII stain. Distribution of elastic fibers in the tumoral interstitium determined by using the elastin–van Gieson stain correlated with maximum attenuation and with the number of small vessels. With these studies, however, the relationship between MER or washout time of contrast material and the histopathologic findings or prognosis was not assessed.

In the present study, the number of microvessels, which were recognized by delineated CD34-positive cells, correlated with the MER. Furthermore, the number of small vessels correlated with the slope value of the time-SI curve, and this number correlated negatively with the T_{max}. These results suggest that pul-

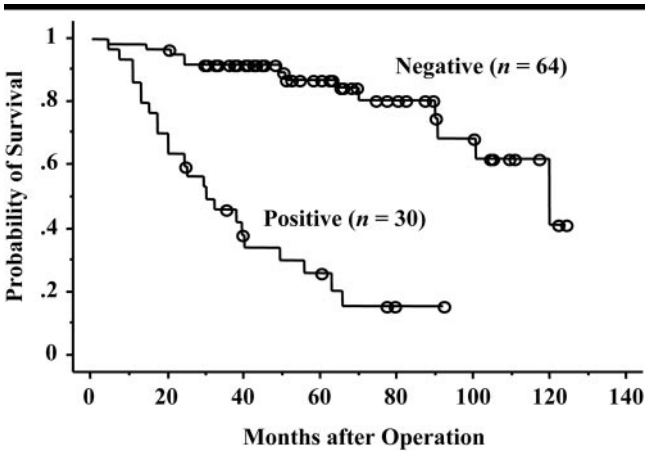

Figure 4. Graph shows survival according to presence or absence of lymph node metastasis. Patients with findings positive for lymph node metastasis *(Positive)* had a significantly shorter overall survival than did those with findings negative for lymph node metastasis *(Negative)* ($P < .0001$).

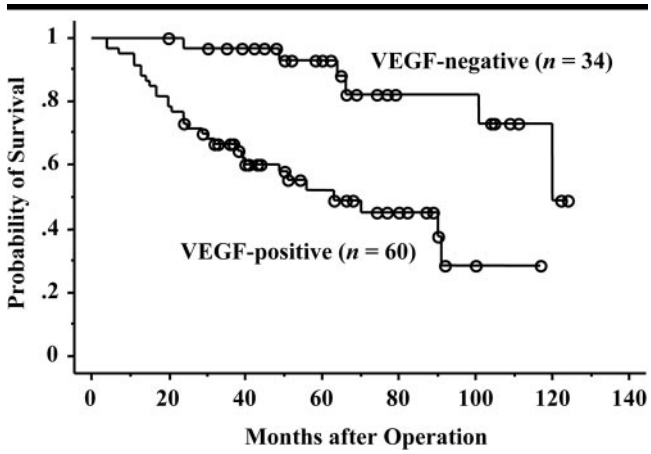

Figure 5. Graph shows survival according to VEGF expression. Patients with VEGF-positive tumors had a significantly shorter overall survival than did those with VEGF-negative tumors ($P < .0001$).

monary carcinomas with many microvessels had stronger and faster gadolinium-based contrast agent enhancement than did pulmonary carcinomas with few microvessels. Because the slope value was calculated from the MER and the T_{max}, the correlation with the microvessel counts and the slope value in the linear regression analysis revealed that both the maximum enhancement and the time correlated with the number of microvessels. The correlation between the washout ratio and the tumor interstitium in the current study suggests that pulmonary carcinomas with a relatively greater amount of interstitial tissue (ie, elastic fibers and collagen fibers) have a smaller washout ratio than do those with less interstitial tissue.

In the present study, we demonstrated that the parameters of the first half of the time-SI curve (ie, MER, T_{max}, and slope value) correlated with tumor angiogenesis (ie, microvessel counts and MVDG), and those of the latter half (ie, washout ratio) correlated with the tumor interstitium (the density grade of elastic fibers and collagen fibers, elastic fibers 1–3 and collagen fibers 1–3). These results suggest that intratumoral circulation of gadopentetate dimeglumine is dependent on the quantity and distribution of microvessels, elastic fibers, and collagen fibers within the tumor. The enhancement characteristics of dynamic MR imaging, therefore, reflect the degree of angiogenesis and neogenesis of the interstitium of pulmonary carcinomas.

Hittmair et al (10) demonstrated that contrast enhancement with iodinated contrast material and with gadopentetate dimeglumine was primarily produced by the accumulation of extravascular contrast material, which is caused both by an increased number of blood vessels and by high vascular permeability. The higher vascularity is caused by faster endothelial proliferation, and the increased vascular permeability is presumed to be caused by various mediators (10).

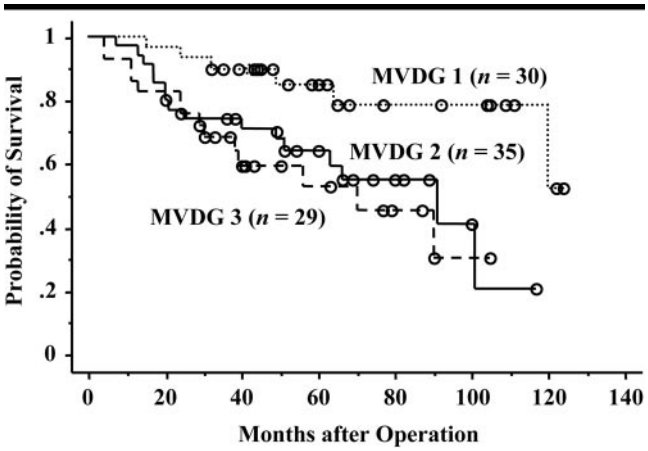

Figure 6. Graph shows survival according to MVDG. Patients with MVDG 1 had a significantly better prognosis than did those with MVDG 2 and 3 (MVDG 1 vs MVDG 2 and 3, $P < .01$). The difference between MVDG 2 and MVDG 3 was not significant.

Experimental evidence suggests that tumor growth depends on angiogenesis (31,32) and that the ingrowth of new capillaries increases the opportunity for tumor cells to enter the circulation. There are reports of a relationship between the intensity of angiogenesis (ie, tumor microvessel counts) and probability of metastasis in various tumors (29,32–35). These reports suggest that the likelihood of metastatic disease increases as the number of intratumoral microvessels increases. Since the number of small vessels had a positive statistical correlation to the MER and a negative correlation to the T_{max}, the results suggest that the probability of metastasis might be increased for patients with pulmonary carcinomas that have strong and early enhancement at MR imaging with gadolinium-based contrast agents.

Angiogenesis, a prerequisite for tumor growth and progression, results from a shift in the equilibrium between angiogenic factor and angiogenic inhibitors (31,36). VEGF is one of the most important factors that mediates angiogenesis for stimulation of endothelial locomotion and proliferation (36). VEGF is

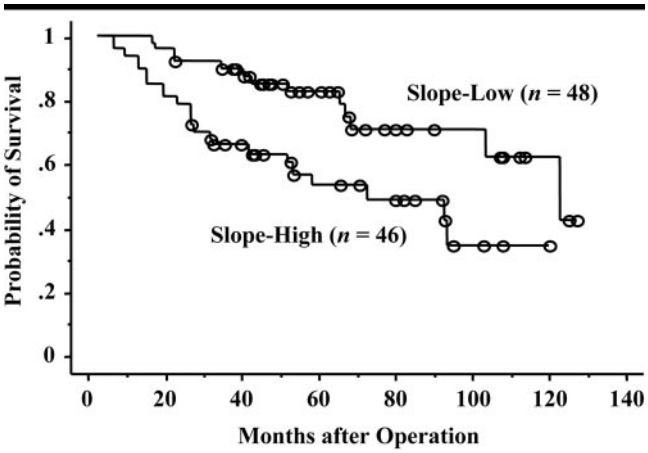

Figure 7. Graph shows survival according to high and low slope value. The cutoff value represents the median of all slope values (37.3% per minute). Patients in the slope-high (>37.3% per minute) group had a significantly worse prognosis than did those in the slope-low (≤37.3% per minute) group ($P < .01$).

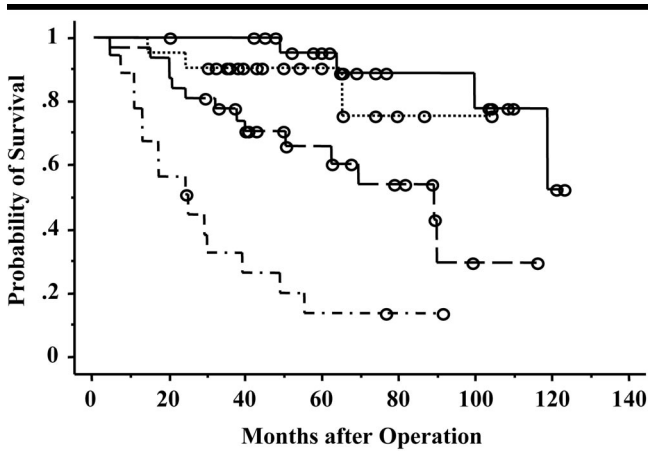

Figure 8. Graph shows survival as a function of zero to three independent factors (ie, VEGF-positive tumor, slope-high [>37.3% per minute] value, and findings positive for lymph node metastasis) derived by using multivariate analysis (log-rank test, $P < .0001$). Solid line = patients without factors, dotted line = patients with one factor, dashed line = patients with two factors, dashed and dotted line = patients with three factors.

found in various types of tumor cells, and its expression is believed to have a pivotal role in the development of tumor blood vessels. Findings in many reports suggested that the microvessel count or the MVDG in cases of VEGF-positive tumors was higher than that in cases of VEGF-negative tumors (12–25). In the present study, VEGF expression of 94 pulmonary carcinomas was evaluated immunohistochemically. The rate of VEGF-positive tumors was 63.8% (adenocarcinoma, 65.7%, vs squamous cell carcinoma, 59.3%; $P = .5601$). The microvessel counts in cases of VEGF-positive tumors were significantly higher than those in cases of VEGF-negative tumors. This finding is consistent with those in previous reports, in addition to dynamic MR imaging characteristics (ie, MER, T_{max}, and slope value), which were correlated with VEGF expression. These correlations suggest that VEGF is one of the major factors concerning angiogenesis, and MR imaging characteristics (especially slope value) might be an indicator for evaluation of VEGF-related tumor angiogenesis in pulmonary carcinomas. Furthermore, MR imaging findings may provide helpful information in the assessment of treatments that target tumor angiogenesis (eg, anti-VEGF agents).

Microvessel counts and VEGF expression have been described as important prognostic factors for non–small cell carcinoma (12–23). In the present study, VEGF expression and MR imaging characteristics (ie, the slope value) were demonstrated to be prognostic factors for small peripheral pulmonary adenocarcinoma and squamous cell carcinoma. However, multivariate analysis showed that high microvessel count–associated poor survival probably is not an independent prognostic factor, because high microvessel counts may result from positive VEGF expression. These results are similar to those of Han et al (37).

Ohta et al (15) and Shibusa et al (16) reported that patients with VEGF-negative tumors had significantly better survival rates than did those with VEGF-positive tumors ($P < .05$) in 17 patients (15) and 44 patients (16) with stage I pulmonary adenocarcinomas. In the present study, VEGF expression and prognosis were reevaluated in 64 patients with stage IA tumors, but the difference between patients with VEGF-positive tumors and VEGF-negative tumors was not statistically significant. Because we studied a different population by using a method that was different from the methods of Ohta et al or Shibusa et al, our results could not be compared with their results. Further evaluation between VEGF expression and the prognosis for stage IA pulmonary carcinoma is needed.

On the other hand, Ohta et al (21) and Fontanini et al (22,23) reported that VEGF expression was associated with hilar and/or mediastinal nodal involvement in pulmonary carcinoma. In the present study, 25 (42%) of 60 patients with VEGF-positive tumors had lymph node metastasis, whereas this occurred in only five (15%) of 34 patients with VEGF-negative tumors ($P < .01$). Patients with VEGF-positive tumors had a greater prevalence of lymph node metastasis than did those with VEGF-negative tumors. Although the detailed mechanisms and the significance of VEGF expression in metastatic lymph nodes remain unknown, the frequency of lymph node metastasis might increase in pulmonary carcinomas that have a large number of microvessels and increased VEGF expression. Because the N factor is the most important prognostic factor, the present result might be due to the presence or absence of lymph node metastasis. Patients with lymph node metastasis had an earlier T_{max} and a higher slope value than did those without metastasis. Moreover, dynamic MR imaging characteristics, especially the slope value, might be useful in assessment of lymph node metastasis because the slope value is correlated with microvessel counts in linear regression analysis, and there is a statistically significant relationship between VEGF expression and the slope value.

In conclusion, the results suggest that intratumoral gadopentetate dimeglumine circulation depends on the quantity and the distribution of small vessels and elastic fibers in the tumoral interstitium. Patients with VEGF-positive tumors, a higher slope value, and positive findings for lymph node metastasis had a significantly shorter overall survival than did those with VEGF-negative tumors, a lower slope value, and findings negative for lymph node metastasis. The highest mortality was seen in patients with all three prognostic factors (15 of 18 [83%]). Findings at dynamic MR imaging might be helpful in the assessment of tumor

angiogenesis and tumor interstitium of pulmonary carcinomas. These findings might also be helpful in the prediction of the prognosis of patients with small peripheral pulmonary carcinomas.

References

1. Swensen SJ, Brown LR, Colby TV, Weaver AL. Pulmonary nodules: CT evaluation of enhancement with iodinated contrast material. Radiology 1995; 194:393–398.
2. Yamashita K, Matsunobu S, Tsuda T, et al. Solitary pulmonary nodule: preliminary study of evaluation with incremental dynamic CT. Radiology 1995; 194:399–405.
3. Yamashita K, Matsunobu S, Takahashi R, et al. Small peripheral lung carcinoma evaluated with incremental dynamic CT: radiologic-pathologic correlation. Radiology 1995; 196:401–408.
4. Swensen SJ, Brown LR, Colby TV, Weaver AL, Midthun DE. Lung nodule enhancement at CT: prospective findings. Radiology 1996; 201:447–455.
5. Zhang M, Kono M. Solitary pulmonary nodules: evaluation of blood flow patterns with dynamic CT. Radiology 1997; 205:471–478.
6. Swensen SJ, Viggiano RW, Midthun DE, et al. Lung nodule enhancement at CT: multicenter study. Radiology 2000; 214: 73–80.
7. Semelka RC, Maycher B, Shoenut JP, Kroeker R, Griffin P, Lertzman M. Dynamic Gd-DTPA enhanced breath-hold 1.5 T MRI of normal lungs and patients with interstitial lung disease and pulmonary nodules: preliminary results. Eur Radiol 1992; 2:576–582.
8. Fujimoto K, Edamitsu O, Meno S, Abe T, Uchida M, Nishimura H. Gd-DTPA-enhanced dynamic MR imaging in pulmonary disease: evaluation of usefulness in differentiating benign from malignant disease (abstr). Radiology 1993; 189(P): 438.
9. Kono M, Adachi S, Kusumoto M, Sakai E. Clinical utility of Gd-DTPA-enhanced magnetic resonance imaging in lung cancer. J Thorac Imaging 1993; 8:18–26.
10. Hittmair K, Eckersberger F, Klepetko W, Helbich T, Herold CJ. Evaluation of solitary pulmonary nodules with dynamic contrast-enhanced MR imaging: a promising technique? Magn Reson Imaging 1995; 13:923–933.
11. Gückel C, Schnabel K, Delmling M, Steinbrich W. Solitary pulmonary nodules: MR evaluation of enhancement patterns with contrast-enhanced dynamic snapshot gradient-echo imaging. Radiology 1996; 200:681–686.
12. Mattern J, Koomagi R, Volm M. Coexpression of VEGF and bFGF in human epidermoid lung carcinomas in associated with increase vessel density. Anticancer Res 1997; 17:2249–2252.
13. Mattern J, Koomagi R, Volm M. Association of vascular endothelial growth factor expression with intratumoral microvessel density and tumor cell proliferation in human epidermoid lung carcinoma. Br J Cancer 1996; 73:931–934.
14. Imoto H, Osaki T, Taga S, Ohgami A, Ichiyoshi Y, Yasumoto K. Vascular endothelial growth factor expression in non-small cell lung cancer: prognostic significance in squamous cell carcinoma. J Thorac Cardiovasc Surg 1998; 115: 1007–1014.
15. Ohta Y, Endo Y, Tanaka M, et al. Significance of vascular endothelial growth factor messenger RNA expression in primary lung cancer. Clin Cancer Res 1996; 2:1411–1416.
16. Shibusa T, Shijubo N, Abe S. Tumor angiogenesis and vascular endothelial growth factor expression in stage I lung adenocarcinoma. Clin Cancer Res 1998; 4:1483–1487.
17. Takahama M, Tsutsumi M, Tsujiuchi T, et al. Frequent expression of the vascular endothelial growth factor in human non-small-cell lung cancers. Jpn J Clin Oncol 1998; 28:176–181.
18. Giatromanolaki A, Koukourakis MI, Kakolyris S, et al. Vascular endothelial growth factor, wild-type p53, and angiogenesis in early operable non-small cell lung cancer. Clin Cancer Res 1998; 4:3017–3024.
19. Takanami I, Tanaka F, Hashizume T, Kodaira S. Vascular endothelial growth factor and its receptor correlate with angiogenesis and survival in pulmonary adenocarcinoma. Anticancer Res 1997; 17:2811–2814.
20. Fontanini G, Boldrini L, Chine S, et al. Expression of vascular endothelial growth factor mRNA in non-small cell lung carcinomas. Br J Cancer 1999; 79: 363–369.
21. Ohta Y, Watanabe Y, Murakami S, et al. Vascular endothelial growth factor and lymph node metastasis in primary lung cancer. Br J Cancer 1997; 76:1041–1045.
22. Fontanini G, Vignati S, Boldrini L, et al. Vascular endothelial growth factor in associated with neovascularization and influences progression of non-small cell lung carcinoma. Clin Cancer Res 1997; 3:861–865.
23. Fontanini G, Vignati S, Lucchi M, et al. Neoangiogenesis and p53 protein in lung cancer: their prognostic role and their relation with vascular endothelial growth factor (VEGF) expression. Br J Cancer 1997; 75:1295–1301.
24. Tateishi U, Nishihara H, Watanabe S, Morikawa T, Abe K, Miyasaka K. Tumor angiogenesis and dynamic CT in lung adenocarcinoma: radiologic-pathologic correlation. J Comput Assist Tomogr 2001; 25:23–27.
25. Fujimoto K, Edamitsu O, Abe T, Meno S, Nishimura H, Hayabuchi N. Small peripheral lung cancer evaluated with dynamic MR imaging: MR-pathologic correlation (abstr). Radiology 1997; 205(P): 675.
26. Mountain CF. Revisions in the international system for staging lung cancer. Chest 1997; 111:1710–1717.
27. Verstraete KL, De Deene Y, Roels H, Dierick A, Uyttendaele D, Kunnen M. Benign and malignant musculoskeletal lesions: dynamic contrast-enhanced MR imaging—parametric "first-pass" images depict tissue vascularization and perfusion. Radiology 1994; 192:835–843.
28. Weidner N, Semple JP, Welch WR, Folkman J. Tumor angiogenesis and metastasis: correlation in invasive breast carcinoma. N Engl J Med 1991; 324:1–8.
29. Buadu LD, Murakami J, Murayama S, et al. Breast lesions: correlation of contrast medium enhancement patterns on MR images with histopathologic findings and tumor angiogenesis. Radiology 1996; 200:639–649.
30. Tomoda M, Maehara Y, Kakeji Y, Ohno S, Ichiyoshi Y, Sugimachi K. Intratumoral neovascularization and growth pattern in early gastric carcinoma. Cancer 1999; 85: 2340–2346.
31. Folkman J, Klagsbrun M. Angiogenetic factors. Science 1987; 235:442–447.
32. Folkman J, Shing Y. Angiogenesis. J Biol Chem 1992; 267:10931–10934.
33. Srivastava A, Laidler P, Davies RP, Horgan K, Hughes LE. The prognostic significance of tumor vascularity in intermediate-thickness (0.76-4.0 mm thick) skin melanoma: a quantitative histologic study. Am J Pathol 1988; 133:419–423.
34. Macchiarini P, Fontanini G, Hardin MJ, Squartini F, Angeletti CA. Relation of neovascularisation to metastasis of non-small-cell lung cancer. Lancet 1992; 340: 145–146.
35. Petruzzelli GJ, Snyderman CH, Johnson JT, Myers EN. Angiogenesis induced by head and neck squamous cell carcinoma xenografts in the chick embryo chorioallantoic membrane model. Ann Otol Rhinol Laryngol 1993; 102:215–221.
36. Cheung N, Wong MP, Yuen ST, Leung SY, Chung LP. Tissue-specific expression pattern of vascular endothelial growth factor isoforms in the malignant transformation of lung and colon. Hum Pathol 1998; 29:910–914.
37. Han H, Silverman JF, Santucci TS, et al. Vascular endothelial growth factor expression in stage I non-small cell lung cancer correlates with neoangiogenesis and a poor prognosis. Ann Surg Oncol 2001; 8:72–29.